Honeycomb oxide heterostructure as a candidate host for a Kitaev quantum spin liquid

Baekjune Kang,[1,*] Miju Park,[1,*] Sehwan Song,[2] Seunghyeon Noh,[3] Daeseong Choe,[3] Minsik Kong,[2] Minjae Kim,[2] Choongwon Seo,[1] Eun Kyo Ko,[4,5] Gangsan Yi,[1,†] Jung-Woo Yoo,[3] Sungkyun Park,[2] Jong Mok Ok,[2,‡] and Changhee Sohn[1,§]

[1]*Department of Physics, Ulsan National Institute of Science and Technology, Ulsan 44919, Republic of Korea*
[2]*Department of Physics, Busan National University, Busan 46241, Republic of Korea*
[3]*Department of Materials Science and Engineering, Ulsan National Institute of Science and Technology, Ulsan 44919, Republic of Korea*
[4]*Center for Correlated Electron Systems, Institute for Basic Science (IBS), Seoul 08826, Republic of Korea*
[5]*Department of Physics and Astronomy, Seoul National University, Seoul 08826, Republic of Korea*

(Received 23 June 2022; revised 21 September 2022; accepted 12 January 2023; published 2 February 2023)

The Kitaev quantum spin liquidand massively quantum entangled states, are so scarce in nature that searching for new candidate systems remains a great challenge. A honeycomb heterostructure could be a promising route to realize and utilize such an exotic quantum phase by providing additional controllability of Hamiltonian and device compatibility, respectively. Here, we provide epitaxial honeycomb oxide thin film $Na_3Co_2SbO_6$, a candidate of Kitaev quantum spin liquid proposed recently. We found a spin glass and antiferromagnetic ground states depending on Na stoichiometry, signifying not only the importance of Na vacancy control but also strong frustration in $Na_3Co_2SbO_6$. Despite its classical ground state, the field-dependent magnetic susceptibility shows remarkable scaling collapse with a single critical exponent, which can be interpreted as evidence of quantum criticality. Its electronic ground state and derived spin Hamiltonian from optical spectroscopy are consistent with the predicted Kitaev model. Our work provides a unique route to the realization and utilization of Kitaev quantum spin liquid.

DOI: 10.1103/PhysRevB.107.075103

I. INTRODUCTION

Quantum entanglement, a subtle nonlocality in nature, becomes a central subject again in the wide range of science and technology [1–4]. Quantum entangled states in many-body condensed matter are particularly interesting as they possess nontrivial topology and fractional excitations, which contributes to the robustness of entanglement against external perturbation [5]. The Kitaev quantum spin liquid (QSL) is a notable example. In this model, spins in a honeycomb lattice are frustrated by the bond-directional Ising interaction, resulting in a massively entangled quantum spin state with fractional Majorana fermions and non-Abelian anyons [6]. Such an exotic phase, however, is so scarce that searching for new candidate materials remains a highly challenging task [7–16].

Being believed to be impossible and barely conducted, heterostructure approaches could be a promising route to realizing and utilizing Kitaev QSL. Every proposed material for Kitaev QSL has classical antiferromagnetic ground states due to the presence of non-Kitaev interaction originating from additional structure distortions or long-range spin interaction [7,12,17]. However, all the existing experiments on Kitaev QSL have been performed in a bulk system, where control of the spin Hamiltonian is limited. In heterostructure geometry, on the other hand, symmetry, strain, and interfacial engineering can be utilized for extensive manipulation of the spin Hamiltonian [18,19]. In addition, we have witnessed the triumphs of heterostructure approaches in semiconductor and spintronic technologies [20]. Therefore, we can expect that similar heterostructure approaches in quantum magnetism can advance breakthroughs in quantum information technology like topological quantum computation.

To utilize heterostructure for Kitaev QSL, however, two major difficulties must be carefully handled. First, most experiments for QSL are bulk-sensitive including inelastic neutron scattering [11] and thermal Hall experiments [14], which can be overcome, however, by performing the newly proposed experiment based on nonlocal spin transport [21]. Second, it remains elusive whether Kitaev QSL candidate materials can be synthesized in heterostructures with minimal disorders or not [22,23]. There have been *zero* studies about the synthesis of Kitaev QSL candidates in heterostructures, with any signs of quantum criticality. In addition, even bulk compounds suffer from disorders, which hinder obtaining intrinsic magnetic and quantum properties of systems [17,24]. It is a common belief that heterostructures are not a suitable platform for quantum magnetism due to more impurities than in bulk.

In this letter, we provide a synthesis of honeycomb oxide heterostructures $Na_3Co_2SbO_6$, a candidate material for Kitaev QSL [15,17,25–31], and experimental signatures of quantum

*These authors contributed equally to this work.
†Deceased.
‡okjongmok@pusan.ac.kr
§chsohn@unist.ac.kr

criticality. We have successfully synthesized stoichiometric, single-phase, and epitaxial $Na_3Co_2SbO_6$ thin films on ZnO substrates. We demonstrate the precise control of Na stoichiometry of the thin film via growth oxygen partial pressure. As we minimized Na vacancies, our thin film shows long-range antiferromagnetic ordering near 8.3 K, the same as the highest reported value in stoichiometric bulk samples. The field-dependent magnetic susceptibility shows remarkable scaling collapse as a function of single variable T/H (T: temperature, H: magnetic field), a signature of quantum criticality. We further conducted optical spectroscopy to reveal the quantitative parameters of the electronic Hamiltonian of the system including charge transfer energy (Δpd), crystal field splitting ($10Dq$), and Hund's coupling (J_H). A constructed spin Hamiltonian from those parameters is consistent with the proposed Kitaev model.

II. EXPERIMENTAL METHODS

Pulsed laser deposition is used to synthesize high-quality $Na_3Co_2SbO_6$ thin films. The O-faced ZnO [0001] were annealed for 1 h at 1100 °C in the ambient pressure. We followed the previously reported synthesis of polycrystalline $Na_3Co_2SbO_6$ powder by solid-state reaction method [25]. The $Na_3Co_2SbO_6$ thin film growth on the treated substrates was performed in a wide range of growth parameters, such as temperature $T = 450 \sim 800$ °C, oxygen partial pressure $P_{O_2} = 0 \sim 2 \times 10^{-1}$ Torr, the energy of the KrF excimer laser ($\lambda = 248\,nm$) $E = 0.9 \sim 2\,\mathrm{J/cm^2}$, and laser repetition rate $2 \sim 10$ Hz. The chamber base pressure was maintained under the 1×10^{-6} Torr. The optimized growth condition was $T = 625$ °C, $P_{O_2} = 0$ mTorr, $E = 0.9\,\mathrm{J/cm^2}$, and laser repetition $= 10$ Hz. The films used to obtain magnetic (optical) properties had a thickness of about 60 (30) nm.

We used a D8 Discovery high-resolution x-ray diffraction (Bruker) with Lynxeye detector to obtain θ-2θ and the rocking curve of $Na_3Co_2SbO_6$ thin film. A superconducting quantum interference device (Quantum Design) is employed to investigate the magnetic properties of $Na_3Co_2SbO_6$ thin films and bare substrate ZnO. The magnetic moment of $Na_3Co_2SbO_6$ is extracted by deducting mass-normalized substrate data. By utilizing an M-2000 ellipsometer (J. A. Woolam Co.), two ellipsometry parameters of $Na_3Co_2SbO_6$ thin film and a bare substrate ZnO were independently measured at room temperature. A two-layer model was used for determining the optical constants of the $Na_3Co_2SbO_6$ thin film.

III. RESULTS AND DISCUSSION

A. Synthesis of $Na_3Co_2SbO_6$ thin film

Among the candidate materials for Kitaev QSL, $Na_3Co_2SbO_6$ could be a promising system for heterostructure approaches as follows. The crystal structure of $Na_3Co_2SbO_6$ is monoclinic layered oxides, where Na^+ layers and $(Co_{2/3}Sb_{1/3}O_2)^-$ layers are alternatively stacked. The Co^{2+} ions in the cobalt-antimony layer construct the honeycomb lattice. Although $Na_3Co_2SbO_6$ has a smaller degree of spin-orbit coupling compared to other candidates like α-$RuCl_3$ and Na_2IrO_3, the $J_{\mathrm{eff}} = 1/2$ state appears as a ground state due to the unquenched orbital momentum of the Co^{2+} [15,28,29]. In addition, the localized $3d$ orbitals and charge-transfer insulating state is favored over extended $4d/5d$ orbitals and Mott insulating state in Kitaev QSL. The localized $3d$ orbital suppresses the undesired next-nearest neighbor exchange interaction and the charge-transfer nature prefers superexchange via oxygen which vanishes the isotropic exchange term in the 90 ° bonding geometry rather than a direct exchange between cobalt ions [32]. Several experiments on bulk $Na_3Co_2SbO_6$ have shown convincing evidence about the presence of strong frustration and large Kitaev exchange terms [15,31]. In particular, it has been theoretically proposed that $Na_3Co_2SbO_6$ can have the Kitaev QSL as a ground state by simply controlling trigonal distortion [29], thereby making $Na_3Co_2SbO_6$ a suitable model system for heterostructure approaches.

The hexagonal substrate ZnO along the [0001] direction provides a good epitaxial relationship with $Na_3Co_2SbO_6$ along the [001] direction, promoting the synthesis of a high-quality thin film. As schematically shown in Fig. 1(a), the hexagonal substrate ZnO (0001) surface exhibits 2D sixfold symmetry with coincident oxygen positions with $Na_3Co_2SbO_6$. Because of similarities in the crystal structure of the $Na_3Co_2SbO_6$ (001) plane and the ZnO (0001) plane, we expect the growth of epitaxial thin films despite the large lattice mismatch between them (∼4.2%). Fig. 1(b) is the x-ray diffraction (XRD) θ-2θ scan of $Na_3Co_2SbO_6$ 60 nm thickness thin film grown on ZnO [0001] substrate by pulsed laser deposition. We observe $00l$ diffraction peaks of $Na_3Co_2SbO_6$ consistent with reported values of single crystals. Fig. 1(c) displays a rocking curve of the $Na_3Co_2SbO_6$ 001 peak. It is fitted by two Lorentzian functions, typically found in relaxed films. The full width at half maximum (0.055 °) of the narrower peak verifies high crystal quality.

B. Na stoichiometry control and evolution of magnetic ground states with Na vacancies

We demonstrate that the sodium stoichiometry of $Na_3Co_2SbO_6$ can be precisely controlled by adjusting the background oxygen partial pressure (P_{O_2}) during the thin film deposition process. Note that, control of sodium stoichiometry has been known to be difficult even in single crystals due to the high reactivity and volatility of sodium ions [17]. As a result, the Néel temperature T_N of powder and single crystals $Na_3Co_2SbO_6$ varies greatly from 4.4 to 8.3 K with different sodium stoichiometry [17,25–27,30]. In the thin-film deposition process, however, we can control the sodium stoichiometry by changing P_{O_2}. According to the previous study on $LiCoO_2$ [33], the number of light elements like Li and Na ions reaching the substrate decreases as the number of collisions with oxygen increases. Fig. 2(a) is the θ-2θ scan near 001 peak of $Na_3Co_2SbO_6$ of different P_{O_2}. As P_{O_2} is increased, the 001 peak shifts to a low angle indicating c-axis elongation. It is consistent with the previous report on Na_xCoO_2 [34], where the c-axis elongated as decreasing x. Fig. 2(b) shows the lattice constants of c^* as a function of different P_{O_2}. We found P_{O_2} below 1 mTorr is required to minimize Na vacancies in heterostructures.

The magnetic ground states of $Na_3Co_2SbO_6$ evolve from antiferromagnetic to spin-glass states with Na vacancies,

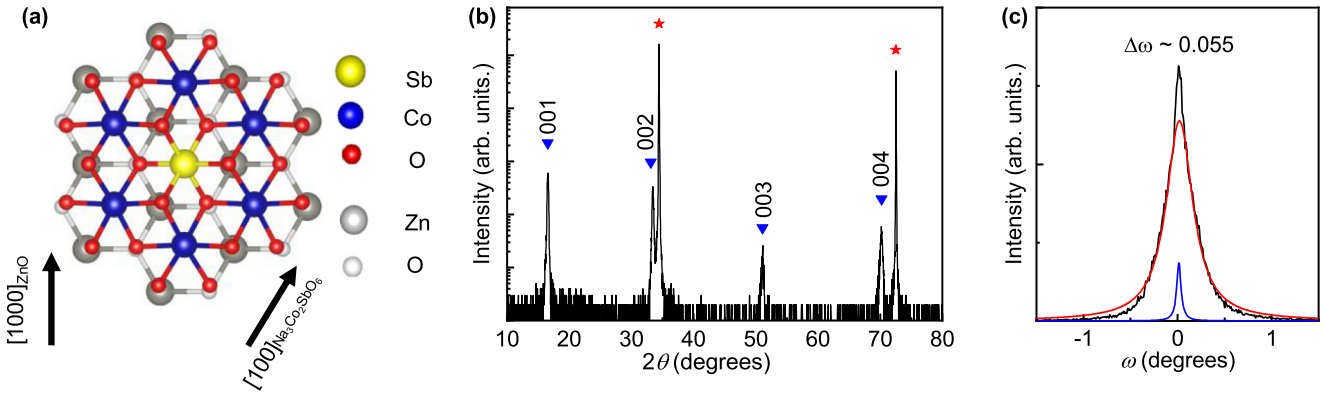

FIG. 1. (a) Schematics of the epitaxial relationship between $Na_3Co_2SbO_6$ (001) and ZnO (0001) atomic planes. (b) XRD θ-2θ data of $Na_3Co_2SbO_6$ thin film grown on ZnO [0001] substrate. The blue triangles and red stars indicate the 00l peaks of $Na_3Co_2SbO_6$ and ZnO, respectively. (c) Rocking curve of 001 peak of $Na_3Co_2SbO_6$ film. The blue and red lines are the fitting functions of two Lorentz oscillators.

indicating not only the importance of Na stoichiometry control but also the existence of strong frustrations in our heterostructures. Fig. 2(c) is the zero-field cooling (ZFC) and field cooling (FC) magnetic susceptibility $\chi(T)$ measured along the Co-Co bonding direction after subtracting the diamagnetic signals from the ZnO substrate. The $\chi(T)$ of the Na-stoichiometric sample grown at $P_{O_2} = 0$ mTorr shows a distinct anomaly at 8.3 K with a negligible bifurcation of ZFC and FC, indicating antiferromagnetic ground states. Note that this temperature is the same as the highest reported value of bulk compounds [17,30]. In a Na-vacant thin film grown at high P_{O_2}, on the other hand, a kink from antiferromagnetic ordering and bifurcation between FC and ZFC becomes weak and conspicuous, respectively, resulting in spin glass states. This observation indicates the control of Na vacancy is essential to identify the true magnetic ground state of $Na_3Co_2SbO_6$. In addition, the emergence of spin glass behavior with small off-stoichiometry implies the presence of strong frustration, a key ingredient for quantum magnetism. The previous theoretical calculation suggests the existence of a subtle balance between ferromagnetic and antiferromagnetic exchange interactions, consistent with the emergence of spin glass states with minimal Na vacancies [29].

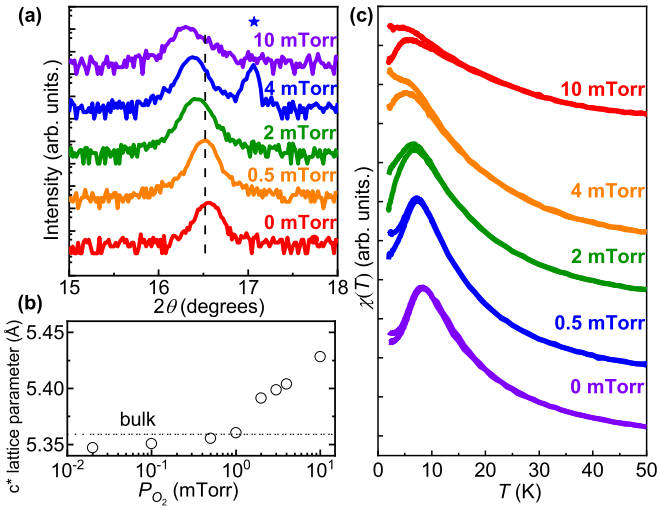

FIG. 2. (a) The P_{O_2} dependence of 001 peak of $Na_3Co_2SbO_6$ thin film. The dashed line is the 001 peak of bulk $Na_3Co_2SbO_6$. The blue star is the forbidden 0001 peak of the ZnO capping layer. (b) The P_{O_2} dependence of c* lattice parameter. The dashed line indicates bulk one. (c) The P_{O_2} dependence of ZFC/FC $\chi(T)$ of $Na_3Co_2SbO_6$.

C. Field-dependent magnetic properties and hidden quantum criticality

The antiferromagnetic ground state in $Na_3Co_2SbO_6$ films is very fragile against an external magnetic field, another evidence of strong frustration and competition of exchange interactions. Fig. 3(a) is in-plane $\chi(T)$ with different applied magnetic fields H. The evident kink at $H = 1$ kOe smeared out as the magnetic field raise over the critical magnetic field around 10 kOe. That suppression of the antiferromagnetic ground state has been observed also in α-$RuCl_3$, a promising candidate of Kitaev QSL. However, the critical field H_c of $Na_3Co_2SbO_6$ is substantially smaller than that of α-$RuCl_3$ despite similar T_N, implying that the system locates closer at the borderlines between ferromagnetic and antiferromagnetic phases. The suppression of antiferromagnetic

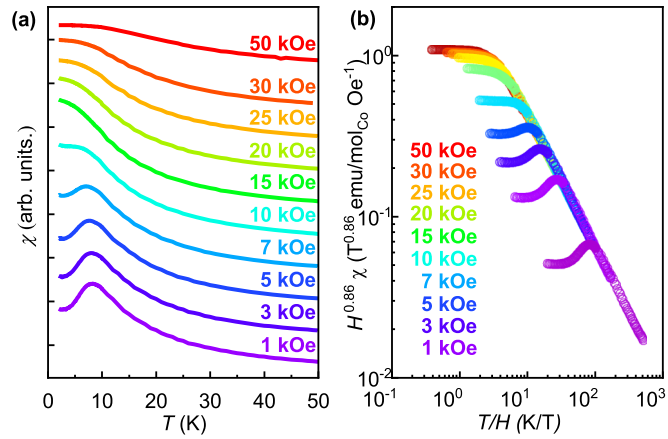

FIG. 3. (a) T-dependent in-plane $\chi(T)$ of $Na_3Co_2SbO_6$ heterostructure at various applied H. (b) Scaling of $H^{0.86}$ $\chi(T)$ as a function T/H on a log-log scale up to $H = 50$ kOe.

ordering observed in our heterostructure is also consistent with recent inelastic neutron scattering on high-quality single crystals that antiferromagnetic ground states evolve into ferrimagnetic and fully polarized states with an applied magnetic field [30].

Despite classical ground states of $Na_3Co_2SbO_6$, we found a remarkable scaling collapse of $\chi(T, H)$ as a function of single variable T/H in all field regions, a signature of quantum criticality. According to previous studies on α-$RuCl_3$, strong quantum fluctuation can be captured in high-temperature phases where thermal fluctuation destroys classical ground states [35,36]. Fig. 3(b) shows the scaling collapse of $H^{0.86}\chi(T, H)$ as a function T/H. $H^{0.86}\chi(T, H)$ converges to a single line in the range 10–50 K where not only Curie-Weiss law is deviated [27] but also the classical ground state is destroyed by thermal fluctuations. The scaling collapse with T/H is in sharp contrast to the classical scaling depending on the reduced temperature $(T - T_c)/T_c$, implying the presence of a quantum critical point at zero kelvin. As a result, such T/H scaling phenomena have been observed in materials close to quantum critical points including heavy-fermion [37] and iron pnictide superconductors [38].

Note that, however, the observed T/H scaling can be also interpreted as a bond-disordered scenario. The bond disorder in spin systems induces power law distribution of antiferromagnetic exchange interactions, resulting in quantum critical like T/H scaling as observed in $Ru_{0.8}Ir_{0.2}Cl_3$ [39] and $H_3LiIr_2O_6$ [40,41]. However, we believe such a scenario does not apply to our system for the following reasons. First, unlike $H_3LiIr_2O_6$ and $Ru_{0.8}Ir_{0.2}Cl_3$ where positions of H and Ir cations are disordered, the $Na_3Co_2SbO_6$ system has ordered Na positions, thereby minimizing disorders in exchange interactions. Second, Na vacancies, the most likely disorders to exist, induce ferromagnetic exchange interactions and make the system spin glass as shown in Fig. 2(c). It is again in contrast to the case of bond-disordered Kitaev spin liquid $Ru_{0.8}Ir_{0.2}Cl_3$, where Ir dopants destablize zigzag long-range orders without spin glass behaviors.

D. Electronic structure and spin Hamiltonian

We further conducted optical spectroscopy on $Na_3Co_2SbO_6$ to extract quantitative parameters for its electronic and spin Hamiltonian. Fig. 4(a) is the real part of optical conductivity $\sigma_1(\omega)$ of the $Na_3Co_2SbO_6$ thin film. Due to the sharp absorption of the ZnO substrate, there is an artificial kink near 3.32 eV highlighted as a blue star. It can be explained by three interband transitions labeled α, β, and γ in the order of increasing energy. We obtained transition energies of those peaks with Lorentz oscillator models; the energies of the three peaks are 4.50 eV (α), 5.36 eV (β), and 6.35 eV (γ). We regard all Lorentz oscillators as interband transitions between the oxygen $2p$ band to the cobalt $3d$ band (p–d transition). Due to the high electrical repulsion among seven electrons in the localized $3d$ band, the U of the Co^{2+} ion is generally higher than the Δ_{pd} [42].

We calculated the energies of optical excitation of d^7 high spin cobalt ion based on the multiorbital Hubbard model. The lowest interband excitations are transitions from oxygen $2p$ to cobalt t_{2g} and e_g orbitals. The final states consisting of

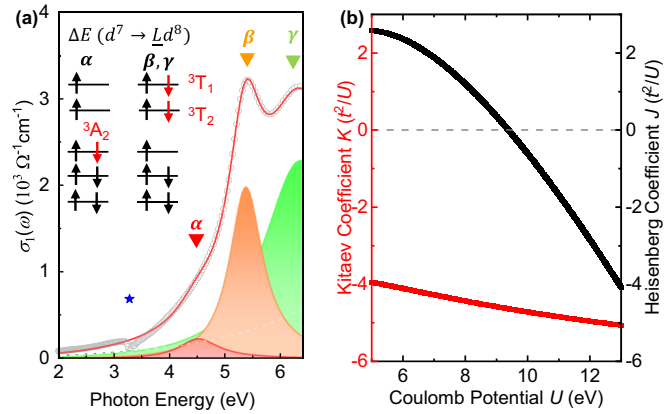

FIG. 4. (a) The real part of optical conductivity $\sigma_1(\omega)$ of $Na_3Co_2SbO_6$. Open circles and solid lines are experimental data and fitting lines with Lorentz oscillators, respectively. The blue star indicates a kink owing to the sharp optical transition in the ZnO substrate. The inset shows the schematic of possible charge-transfer transitions of $t_{2g}^5 e_g^2$ electron configuration. The red arrows represent excited electrons from O $2p$ orbitals. (b) Calculated the Heisenberg coefficient J and the Kitaev coefficient K in the units of t^2/U.

two holes are equivalent to those consisting of two electrons due to electron-hole symmetry. We calculated the expected electrostatic energies of each wave function. After the electron is optically excited from oxygen $2p$ to cobalt $3d$ band, the highest magnetic quantum number wave functions constituted by two holes are described as [43]

$$\begin{aligned} |\Psi(ee^3A_2)(\boldsymbol{r_1}, \boldsymbol{r_2})\rangle &= |u_\uparrow(\boldsymbol{r_1})v_\uparrow(\boldsymbol{r_2})|, \\ |\Psi(te^3T_1)(\boldsymbol{r_1}, \boldsymbol{r_2})\rangle &= |\xi_\uparrow(\boldsymbol{r_1})u_\uparrow(\boldsymbol{r_2})|, \\ |\Psi(te^3T_2)(\boldsymbol{r_1}, \boldsymbol{r_2})\rangle &= |\xi_\uparrow(\boldsymbol{r_1})v_\uparrow(\boldsymbol{r_2})|, \end{aligned} \tag{1}$$

where $\xi_\uparrow = d_{xy}, d_{yz}, d_{zx}, u_\uparrow = d_{3z^2-r^2}, v_\uparrow = d_{x^2-y^2}$ orbital with up-spin, $|\ |$ is slater determinant satisfying the antisymmetric nature of fermion, t/e is a hole in t_{2g}/e_g manifold, $^3A_2$, $^3T_1$, $^3T_2$ is the symmetry of wave function. All wave functions are a triplet ($l = 1$), and there are three wave functions according to the magnetic quantum number. Due to the degeneracy of three wave functions, we choose the easiest one to compute. The expectation energy for the Coulomb Hamiltonian of each wav efunction is written as

$$\begin{aligned} \langle\Psi(ee^3A_2)|\frac{1}{r}|\Psi(ee^3A_2)\rangle &= A - 8B, \\ \langle\Psi(te^3T_2)|\frac{1}{r}|\Psi(te^3T_2)\rangle &= A - 8B, \\ \langle\Psi(te^3T_1)|\frac{1}{r}|\Psi(te^3T_1)\rangle &= A + 4B, \end{aligned} \tag{2}$$

where A, B, and C are called the Racah parameter. The Racah parameter is the function of slater integrals F^k

$$F^k = \int_0^\infty \boldsymbol{r}_1^2 d\boldsymbol{r}_1 \int_0^\infty \boldsymbol{r}_2^2 d\boldsymbol{r}_2 R^2(\boldsymbol{r}_1) R^2(\boldsymbol{r}_2) \frac{\boldsymbol{r}_<^{\boldsymbol{k}}}{\boldsymbol{r}_>^{\boldsymbol{k}+1}}, \tag{3}$$

where $R(r)$ is normalized radial part of the $3d$ orbital, $r_< = \min\{r_1, r_2\}$, $r_< = \max\{r_1, r_2\}$. The Slater integral is simplified as $F_0 = F^0$, $F_2 = F^2/49$, $F_4 = F^4/441$. The Racah

parameter is written as

$$A = F_0 - 49F_4, \quad B = F_2 - 5F_4, \quad C = 35F_4. \tag{4}$$

For the $3d$ electron, $5B \approx C$ satisfies Ref. [28]. The Hund's coupling is also written as the Racah parameter, $J_H = 3B + C \approx 8B$. Consequently, the energies of optical excitation are expressed as

$$E(^3A_2) = \Delta_{pd},\ E(^3T_2) = \Delta_{pd} + 10Dq,\ E(^3T_1) = \Delta_{pd} + 10Dq + \tfrac{3}{2}J_H, \tag{5}$$

where Δ_{pd} is charge-transfer energy.

We extract the quantitative parameters for electronic structures of $Na_3Co_2SbO_6$ from the multiorbital Hubbard model. The inset of Fig. 4(a) represents the three possible p-d transitions in the high spin $3d^7$ system (Co^{2+}). The lowest transition is from O $2p$ to Co t_{2g} orbitals ($^3A_2$ symmetry), whose energy is defined by Δ_{pd}. The other two transitions are from O $2p$ to Co e_g orbitals. Because of different orbital overlaps in the final state ($^3T_1$ and $^3T_2$ symmetry), each excitation requires different energies, $\Delta_{pd} + 10Dq$ ($^3T_2$) and $\Delta_{pd} + 10Dq + 3/2J_H$ ($^3T_1$). Based on the multiorbital Hubbard model, we assigned peaks α, β, and γ as $^3A_2$, $^3T_1$, and $^3T_2$ transitions. From the above equations, we calculate the quantitative value of three electronic parameters, Δ_{pd}, $10Dq$, and J_H to 4.50, 0.86, and 0.66 eV, respectively.

We reconstruct the spin Hamiltonian of $Na_3Co_2SbO_6$ based on electronic structure parameters by following the previous theoretical spin model [28]. The spin-exchange Hamiltonian of $Na_3Co_2SbO_6$ without trigonal distortion is written as

$$H = J\sum_{\langle ij\rangle} S_i \cdot S_j + K\sum_{\langle ij\rangle, a=\mathrm{b}} S_i^a S_j^b + \Gamma \sum_{\langle ij\rangle, a\neq \mathrm{b}} S_i^a S_j^b, \tag{6}$$

where J, K, and Γ are the isotropic Heisenberg coefficient, anisotropic Kitaev coefficient, and off-diagonal term, respectively. The J, K, and Γ are the function of the electronic parameters, Δ_{pd}, $10Dq$, J_H, and U. Due to $\Gamma \sim 0.001\,K$ in the $U > 5$ eV range, we only calculate J and K based on the spin-exchange interaction model of the $3d^7$ cobalt compound without trigonal distortion. Fig. 4(b) exhibits the J and K as a function of U with a unit of t^2/U. We follow the calculation in the previous report with (Δ_{pd}, $10Dq$, J_H) = (4.50, 0.86, and 0.66 eV) obtained above [28]. We found that J becomes close to zero with $U \sim 9.5$ eV. According to the previous photoemission study on CoO [44], U of Co $3d$ orbitals was estimated as $9 \sim 11$ eV. Therefore, our spectroscopic approaches imply that the spin Hamiltonian of $Na_3Co_2SbO_6$ heterostructures can be possibly described by Kitaev physics if the trigonal distortion is suppressed.

IV. SUMMARY

In summary, we provided epitaxial honeycomb oxide heterostructure $Na_3Co_2SbO_6$ with signatures of quantum criticality. Its electronic and magnetic properties can be explained in terms of the proposed Kitaev physics. The controllability and device compatibilities heterostructure provides could be a promising route to the future realization and application of the Kitaev phases. For example, providing $Na_3Co_2SbO_6$ heterostructures will enable us to engineer the trigonal crystal field, the major source of the antiferromagnetic ordering in $Na_3Co_2SbO_6$. Using isotropic substrates could also help to reduce the orthorhombic distortions existing in bulk $Na_3Co_2SbO_6$ as well [30]. Besides Kitaev physics, honeycomb oxide heterostructures have been proposed for a variety of correlated topological phases [45]. The demonstration of the successful growth of honeycomb oxides, therefore, will promote further searching for topological insulators and quantum anomalous Hall insulators in strongly correlated electron systems.

ACKNOWLEDGMENTS

We thank E.-G. Moon and J. Kim for the fruitful discussion. This work is mainly supported by the National Research Foundation (NRF) funded by the Ministry of Science and ICT(2020R1C1C1008734) and Creative Materials Discovery Program through the National Research Foundation of Korea (NRF) funded by the Korean government (MSIT) (2017M3D1A1040834). J.M.O. acknowledges a grant from the Korea Basic Science Institute (National research Facilities and Equipment Center) funded by the Ministry of Education (Grant No. 2021R1A6C101A429) and a grant from the National Research Foundation of Korea (NRF) funded by the Korean government (MSIT) (No. 2021R1F1A1056934). E.K.K. is supported by Research Center Program of the Institute for Basic Science of Korea (Grant no. IBS-R009-D1). The Excimer Laser COMPexPro 201F (Coherent Co.) for thin film growth and M-2000 ellipsometer (J.A.Woolam Co.) for optical measurements are supported by the IBS Center for Correlated Electron systems, Seoul National University.

B.K., M.P., G.Y., and C.S. conceptualized this work. B.K. and M.P. synthesized and characterized the thin films. S.S., S.N., D.C., M.K., and M.K. performed and assisted in the magnetic property experiments. M.K. and M.K. synthesized polycrystalline targets for pulsed laser deposition. B.K. and E.K.K. performed optical spectroscopy. B.K., M.P., C.S., J.-W.Y., S.P., J.M.O., and C.S. analyzed the experimental data. B.K. and C.S. wrote the paper with input from all coauthors.

[1] K. Satzinger, Y.-J. Liu, A. Smith, C. Knapp, M. Newman, C. Jones, Z. Chen, C. Quintana, X. Mi, A. Dunsworth *et al.*, Science **374**, 1237 (2021).

[2] G. Semeghini, H. Levine, A. Keesling, S. Ebadi, T. T. Wang, D. Bluvstein, R. Verresen, H. Pichler, M. Kalinowski, R. Samajdar *et al.*, Science **374**, 1242 (2021).

[3] K. K. Mehta, C. D. Bruzewicz, R. McConnell, R. J. Ram, J. M. Sage, and J. Chiaverini, Nat. Nanotechnol. **11**, 1066 (2016).

[4] H.-S. Zhong, H. Wang, Y.-H. Deng, M.-C. Chen, L.-C. Peng, Y.-H. Luo, J. Qin, D. Wu, X. Ding, Y. Hu *et al.*, Science **370**, 1460 (2020).

[5] C. Nayak, S. H. Simon, A. Stern, M. Freedman, and S. DasSarma, Rev. Mod. Phys. **80**, 1083 (2008).

[6] A. Kitaev, Ann. Phys. **321**, 2 (2006).

[7] Y. Singh, S. Manni, J. Reuther, T. Berlijn, R. Thomale, W. Ku, S. Trebst, and P. Gegenwart, Phys. Rev. Lett. **108**, 127203 (2012).

[8] T. Takayama, A. Kato, R. Dinnebier, J. Nuss, H. Kono, L. S. I. Veiga, G. Fabbris, D. Haskel, and H. Takagi, Phys. Rev. Lett. **114**, 077202 (2015).

[9] Y. Yamaji, T. Suzuki, T. Yamada, S.-i. Suga, N. Kawashima, and M. Imada, Phys. Rev. B **93**, 174425 (2016).

[10] M. Abramchuk, C. Ozsoy-Keskinbora, J. W. Krizan, K. R. Metz, D. C. Bell, and F. Tafti, J. Am. Chem. Soc. **139**, 15371 (2017).

[11] A. Banerjee, J. Yan, J. Knolle, C. A. Bridges, M. B. Stone, M. D. Lumsden, D. G. Mandrus, D. A. Tennant, R. Moessner, and S. E. Nagler, Science **356**, 1055 (2017).

[12] A. Banerjee, P. Lampen-Kelley, J. Knolle, C. Balz, A. A. Aczel, B. Winn, D. Pajerowski, J. Yan, C. A. Bridges, A. T. Savici *et al.*, npj Quantum Mater. **3**, 8 (2018).

[13] K. Geirhos, P. Lunkenheimer, M. Blankenhorn, R. Claus, Y. Matsumoto, K. Kitagawa, T. Takayama, H. Takagi, I. Kézsmárki, and A. Loidl, Phys. Rev. B **101**, 184410 (2020).

[14] T. Yokoi, S. Ma, Y. Kasahara, S. Kasahara, T. Shibauchi, N. Kurita, H. Tanaka, J. Nasu, Y. Motome, C. Hickey *et al.*, Science **373**, 568 (2021).

[15] C. Kim, J. Jeong, G. Lin, P. Park, T. Masuda, S. Asai, S. Itoh, H.-S. Kim, H. Zhou, J. Ma, and J.-G. Park, J. Phys. Condens. Matter **34**, 045802 (2021).

[16] K. Hwang, A. Go, J. H. Seong, T. Shibauchi, and E.-G. Moon, Nat. Commun. **13**, 323 (2022).

[17] J.-Q. Yan, S. Okamoto, Y. Wu, Q. Zheng, H. D. Zhou, H. B. Cao, and M. A. McGuire, Phys. Rev. Mater. **3**, 074405 (2019).

[18] S. I. Csiszar, M. W. Haverkort, Z. Hu, A. Tanaka, H. H. Hsieh, H.-J. Lin, C. T. Chen, T. Hibma, and L. H. Tjeng, Phys. Rev. Lett. **95**, 187205 (2005).

[19] E.-J. Guo, R. D. Desautels, D. Keavney, A. Herklotz, T. Z. Ward, M. R. Fitzsimmons, and H. N. Lee, Phys. Rev. Mater. **3**, 014407 (2019).

[20] M. N. Baibich, J. M. Broto, A. Fert, F. Nguyen Van Dau, F. Petroff, P. Etienne, G. Creuzet, A. Friederich, and J. Chazelas, Phys. Rev. Lett. **61**, 2472 (1988).

[21] T. Minakawa, Y. Murakami, A. Koga, and J. Nasu, Phys. Rev. Lett. **125**, 047204 (2020).

[22] M. Jenderka, J. Barzola-Quiquia, Z. Zhang, H. Frenzel, M. Grundmann, and M. Lorenz, Phys. Rev. B **88**, 045111 (2013).

[23] M. Jenderka, R. Schmidt-Grund, M. Grundmann, and M. Lorenz, J. Appl. Phys. **117**, 025304 (2015).

[24] M. Yamashita, J. Gouchi, Y. Uwatoko, N. Kurita, and H. Tanaka, Phys. Rev. B **102**, 220404(R) (2020).

[25] L. Viciu, Q. Huang, E. Morosan, H. Zandbergen, N. Greenbaum, T. McQueen, and R. Cava, J. Solid State Chem. **180**, 1060 (2007).

[26] C. Wong, M. Avdeev, and C. D. Ling, J. Solid State Chem. **243**, 18 (2016).

[27] M. I. Stratan, I. L. Shukaev, T. M. Vasilchikova, A. N. Vasiliev, A. N. Korshunov, A. I. Kurbakov, V. B. Nalbandyan, and E. A. Zvereva, New J. Chem. **43**, 13545 (2019).

[28] H. Liu and G. Khaliullin, Phys. Rev. B **97**, 014407 (2018).

[29] H. Liu, J. Chaloupka, and G. Khaliullin, Phys. Rev. Lett. **125**, 047201 (2020).

[30] X. Li, Y. Gu, Y. Chen, V. O. Garlea, K. Iida, K. Kamazawa, Y. Li, G. Deng, Q. Xiao, X. Zheng, Z. Ye, Y. Peng, I. A. Zaliznyak, J. M. Tranquada, and Y. Li, Phys. Rev. X **12**, 041024 (2022).

[31] A. L. Sanders, R. A. Mole, J. Liu, A. J. Brown, D. Yu, C. D. Ling, and S. Rachel, Phys. Rev. B **106**, 014413 (2022).

[32] G. Jackeli and G. Khaliullin, Phys. Rev. Lett. **102**, 017205 (2009).

[33] T. Ohnishi and K. Takada, Appl. Phys. Express **5**, 055502 (2012).

[34] L. Cui, Y. Zhao, G. Zhang, W. Zhang, Z. Guo, W. Ren, X. Zhang, and M. Zhu, J. Alloys Compd. **426**, 72 (2006).

[35] H. Li, D.-W. Qu, H.-K. Zhang, Y.-Z. Jia, S.-S. Gong, Y. Qi, and W. Li, Phys. Rev. Res. **2**, 043015 (2020).

[36] S. M. Winter, K. Riedl, D. Kaib, R. Coldea, and R. Valentí, Phys. Rev. Lett. **120**, 077203 (2018).

[37] A. Schröder, G. Aeppli, R. Coldea, M. Adams, O. Stockert, H. Löhneysen, E. Bucher, R. Ramazashvili, and P. Coleman, Nature (London) **407**, 351 (2000).

[38] I. M. Hayes, R. D. McDonald, N. P. Breznay, T. Helm, P. J. Moll, M. Wartenbe, A. Shekhter, and J. G. Analytis, Nat. Phys. **12**, 916 (2016).

[39] S.-H. Do, C. H. Lee, T. Kihara, Y. S. Choi, S. Yoon, K. Kim, H. Cheong, W.-T. Chen, F. Chou, H. Nojiri, and K.-Y. Choi, Phys. Rev. Lett. **124**, 047204 (2020).

[40] R. Yadav, R. Ray, M. S. Eldeeb, S. Nishimoto, L. Hozoi, and J. van den Brink, Phys. Rev. Lett. **121**, 197203 (2018).

[41] Y. Li, S. M. Winter, and R. Valentí, Phys. Rev. Lett. **121**, 247202 (2018).

[42] G. Lee and S.-J. Oh, Phys. Rev. B **43**, 14674 (1991).

[43] S. Sugano, *Multiplets of Transition-Metal Ions in Crystals* (Elsevier, Amsterdam, 2012).

[44] Z.-X. Shen, J. W. Allen, P. A. P. Lindberg, D. S. Dessau, B. O. Wells, A. Borg, W. Ellis, J. S. Kang, S.-J. Oh, I. Lindau, and W. E. Spicer, Phys. Rev. B **42**, 1817 (1990).

[45] S. Raghu, X.-L. Qi, C. Honerkamp, and S.-C. Zhang, Phys. Rev. Lett. **100**, 156401 (2008).